

Development of a finite element model of high energy laser-material interaction

Matthew Ross and Dan Pope

Dstl Porton Down, Salisbury, SP4 0JQ, UK

1 Abstract

A thermomechanical modelling technique was developed using LS-DYNA for simulating the heating and subsequent erosion of metallic elements by a continuous wave laser beam. Accurate representation of the laser-material interaction requires inclusion of several physical phenomena:

- Heating via absorption of the laser beam;
- Radiative cooling;
- Convective cooling;
- Thermal conduction;
- Mass loss by phase change.

To model heating via absorption of the laser beam, the use of the recently implemented LS-DYNA keyword, ***BOUNDARY_FLUX_TRAJECTORY**, is required. When modelling the phenomenon of “burn-through”, the above keyword was applied along with ***BOUNDARY_CONVECTION** and ***BOUNDARY_RADIATION**, to update the transient surface heat flux condition upon element erosion (facilitated by ***MAT_ADD_EROSION**). Predictions from the modelling technique were compared against test data from experiments focused on the thermal loading of flat steel plates with differing laser beam powers. The modelling technique showed good correlation with the measured data and is considered validated for simulating laser heating under a limited range of parameters. The technique also has potential for further development with the incorporation of additional physical phenomena and more complex geometries.

2 Introduction

Laser processing of materials is an expanding technical field, servicing a broad range of applications, including: additive manufacturing, cutting, and welding [1-3]. LS-DYNA has several capabilities important for modelling these phenomena:

- It can solve coupled thermal-mechanical problems;
- It is not interrupted by the deletion of solid or surface elements;
- Surface heat fluxes can be inherited by surfaces that are newly exposed when elements are deleted.

The keyword ***BOUNDARY_FLUX_TRAJECTORY** is essential for modelling such problems, as it possesses several unique features that correspond well to the surface conditions imposed by a continuous wave high energy laser.

3 New Keyword, ***BOUNDARY_FLUX_TRAJECTORY**

The keyword ***BOUNDARY_FLUX_TRAJECTORY** (introduced in LS-DYNA Manual R12) is used to apply a surface heat flux on to a segment set for either a shell or solid structure. It can be used in either a “thermal” only or a “coupled thermal-structural” solution (***CONTROL_SOLUTION**, SOLN = 1 or 2). The cards for this keyword are listed in Table 1 below.

	1	2	3	4	5	6	7	8
Card 1	SSID	PSEROD	NSID1	SPD1	NSID2	SPD2	RELVEL	
Card 2	EROD	LOC	LCROT	LCLAT				
Card 3	IFORM	LCTIM	Q	LCINC	ENFOR			
Card 4	P1	P2	P3	P4	P5	P6	P7	P8
Card 5	TX	TY	TZ					

Table 1: Keydeck entry for *BOUNDARY_FLUX_TRAJECTORY

The use of *BOUNDARY_FLUX_TRAJECTORY has several requirements:

1. A segment set is needed, using the keyword *SET_SEGMENT. This will be assigned to the surface area that the laser heat flux is initially applied to. *BOUNDARY_FLUX_TRAJECTORY will automatically create new segments on newly exposed surfaces as elements are eroded. The set ID is the input for SSID.
2. A part set is needed, using the keyword *SET_PART. This can be formed of one or more parts. The set ID is the input for PSEROD.
3. A node set is needed, using the keyword *SET_NODE. This is the nodal path that the center of the laser travels along. At least two nodes are required and they should be part of the same surface as the segment set. The set ID is the input for NSID1.
4. A speed for the laser needs to be defined, using SPD1. In this instance the laser is stationary and the default value for SPD1 is 0, so no input was required. A moving laser will require values for SPD1.
5. An aiming direction for the laser needs to be defined. This can be done by using NSID2 and SPD2 for a variable direction, or using TX, TY and TZ for a constant direction.
6. EROD is set to 1 (default value is 0) so that heat fluxes are inherited by newly exposed surfaces when elements are deleted.
7. In this case the laser heat fluxes have a Gaussian distribution, so IFORM needs to be set to 2.
8. The total power from the laser is defined by Q. The units for power are dependent on the length, mass and time units used for the model.
9. ENFOR accounts for the angle of incidence between the laser direction and the exposed surfaces. Without this, scaling problems occur with the total laser power when elements are eroded. A value of 1 for ENFOR is sufficient in this case.
10. The Gaussian distribution is characterised by the values of P1 through to P6. How these relate to a Gaussian distribution is explained in Table 2.

All other inputs from Table 1, not in the above requirements, can be utilized for different scenarios but are not essential.

4 Physical Phenomena and LS-DYNA Functionality

4.1 Laser Heat Flux

Incident radiation from a laser is either reflected, absorbed or transmitted [4] as shown by Fig. 1 and Eq.1.

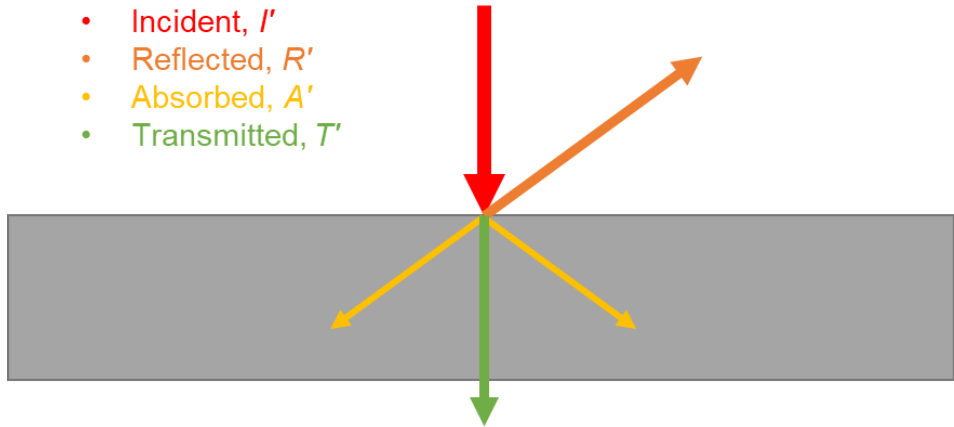


Fig. 1: Interaction of radiation with solid

$$I' = R' + A' + T' \quad (1)$$

In the case of an opaque solid such as steel, T' will be equal to zero and all incident radiation will either be absorbed or reflected as described in Eq. 2.

$$T' = 0; I' = R' + A' \quad (2)$$

The ratio of A' to I' is referred to as the absorptivity, α . This quantifies the amount of energy absorbed and is always a value between 0 and 1. With a given incident laser power intensity of I , the surface heat flux from the laser (q''_{laser}) is given by Eq. 3.

$$q''_{laser} = I \times \alpha \quad (3)$$

The spatial distribution of the laser power intensity, I , can in this case be represented by a Gaussian distribution, which is one of the key reasons for using `*BOUNDARY_FLUX_TRAJECTORY`. Combining Eq. 3 with a 2D Gaussian distribution function yields the following equation for calculating q''_{laser} as a function of radius r .

$$q''_{laser} = \frac{q \times \alpha}{2 \times \pi \times s^2} \exp\left(-\frac{r^2}{2 \times s^2}\right) \quad (4)$$

The constants for Eq.4 are the total laser power q , the absorptivity α and the standard deviation s .

Two graphical examples for a q of 1000 W are shown in Fig. 2 below.

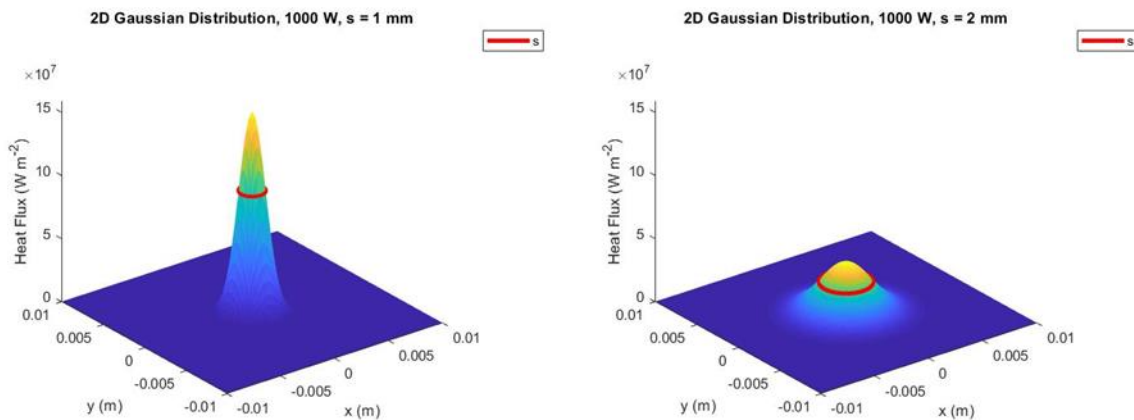


Fig. 2: Heat flux densities using Gaussian distributions

Table 2 below lists inputs for defining Gaussian distributions using ***BOUNDARY_FLUX_TRAJECTORY** and shows how these parameters align with inputs for Eq. 4. For a simple axisymmetric Gaussian distribution some values appear redundant (for example there are three separate inputs for the standard deviation), however they offer useful versatility when defining more complex spatial heat flux distributions that differ from an axisymmetric Gaussian distribution.

Input in *BOUNDARY_FLUX_TRAJECTORY	Variable or Constant?	Variable Name
Q	Variable	Product of Absorptivity and Total laser power, $q \times \alpha$
P1	Variable	Standard deviation, s
P2	Variable	Standard deviation, s
P3	Variable	Standard deviation, s
P4	Constant of 1.0	N/A
P5	Constant of 1.0	N/A
P6	Constant of 0.5	N/A

Table 2: Example input for a Gaussian distribution

In this case α was assumed to be constant, however it can vary with different conditions. For applying a variable α , some additional inputs from Table 1 can be useful. For example, LCTIM can be used to vary α with time and LCINC can be used to vary α with angle of incidence.

4.2 Re-radiation

The amount of energy lost from a surface by thermal radiation, q''_{rerrad} , is quantified by the Stefan-Boltzmann equation as shown in Eq. 5 below.

$$q''_{rerrad} = \varepsilon \times \sigma \times (T_{amb}^4 - T_{surf}^4) \quad (5)$$

The variables of the equation are the Stefan-Boltzmann constant σ , the surface and ambient temperatures in Kelvin (T_{amb} and T_{surf}) and the emissivity ε . According to Kirchoff's Laws of Thermal Radiation [5], both α and ε are considered equal for a given radiation wavelength λ , when temperature T and angle of incidence θ are the same. This gives the relationship between α and ε displayed in Eq. 6 below.

$$\alpha_{\lambda}(\theta, T) = \varepsilon_{\lambda}(\theta, T) \quad (6)$$

However, this rule is not applicable considering radiation absorbed from the laser will be predominantly of a single wavelength and radiation emitted from the target surface will be on a wavelength distribution defined by Planck's Law [5]. Hence, two separate values are required in this scenario for α and ε .

The keyword for applying this surface heat flux in LS-DYNA is ***BOUNDARY_RADIATION_SET**. The application is straightforward [6] and PSEROD has been added to this keyword so the heat flux boundary condition is inherited by newly exposed surfaces when elements are eroded. Multiple instances of this keyword using the same PSEROD should be avoided, as this will result in the boundary condition being applied multiple times to the same surface.

4.3 Convection

The amount of energy lost from a surface by contact with an external fluid is called convection, q''_{conv} , and is quantified by Eq. 7 below.

$$q''_{conv} = h(T_{amb} - T_{surf}) \quad (7)$$

Similar to Eq. 5, the new variable in Eq. 7 is the convective heat transfer coefficient h . This was set as $10 \text{ W m}^{-2} \text{ K}^{-1}$, a typical value for convection in air with no forced convection.

The keyword for applying this surface heat flux in LS-DYNA is `*BOUNDARY_CONVECTION_SET`. The application is similar to `*BOUNDARY_RADIATION_SET` and is very straightforward [6].

4.4 Material Model

The erosion of solid elements to represent melting requires the use of the keyword `*MAT_ADD_EROSION`. This keyword only functions with a mechanical solution, so a coupled thermal structural solution is required for laser-induced erosion by default. The only input required is `MXTMP` for the melting point, which sets the temperature above which elements are deleted.

Both a thermal material model and a structural material model were required for the coupled solution. These were `*MAT_THERMAL_ISOTROPIC_TD_LC` and `*MAT_ELASTIC_PLASTIC_THERMAL` respectively.

The latent heat of fusion ΔH_f was applied using the heat capacity values contained within the thermal material model. To represent the enthalpy required for the solid to liquid phase change, an addition is made to the heat capacity values before the melting point temperature. The thermal material model `*MAT_THERMAL_ISOTROPIC_PHASE_CHANGE` can be used to automatically make this addition to heat capacity data that does not already include the ΔH_f .

5 Model Set-Up

The LS-DYNA modelling technique was tested using data from a set of three experiments. Each experiment involved a flat plate of mild steel being heated by a high energy laser to the point where the laser fully penetrated the target, cutting a hole through its centre.

The same mesh of 8-node solid elements was used for all three models, representing the mild steel target. Element resolution was refined around the central region of the mesh, allowing transient heating and thermal stress to be accurately captured, and graded to larger elements moving away from the centre, for computational economy.

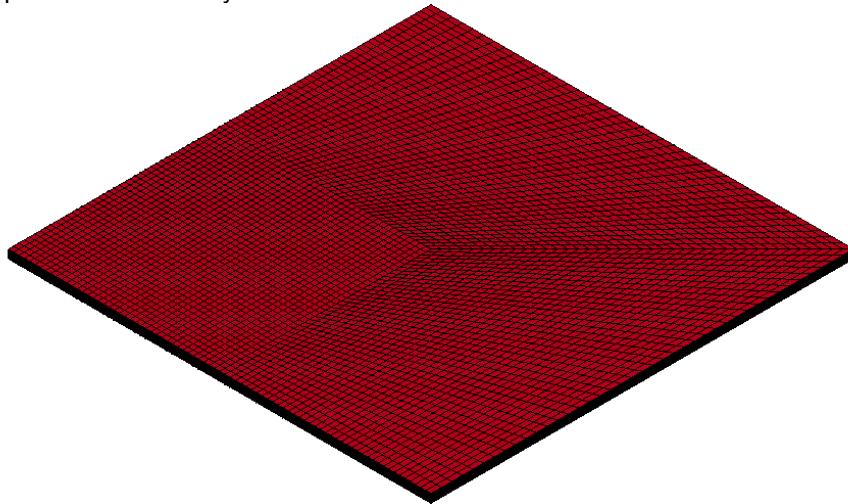


Fig. 3: Finite element mesh

To further improve model efficiency, the scenario was modelled in quarter symmetry, with appropriate boundary conditions being assigned along the symmetry axes. A comparison of the quarter symmetry mesh in Fig. 3 and a mesh explicitly representing the entire system showed no difference in output.

There were a total of 48,000 solid elements in the mesh, with a thickness of 10 solid elements in the z-direction. Including the boundary and symmetry edges, there were a total of 12,000 element faces forming the exterior of the mesh.

To represent a fixed condition, the periphery of the plate was constrained against movement in the x, y and z directions (as shown in Fig. 4). The lines of quarter symmetry were constrained in the x or y directions only. No mechanical loads were applied.

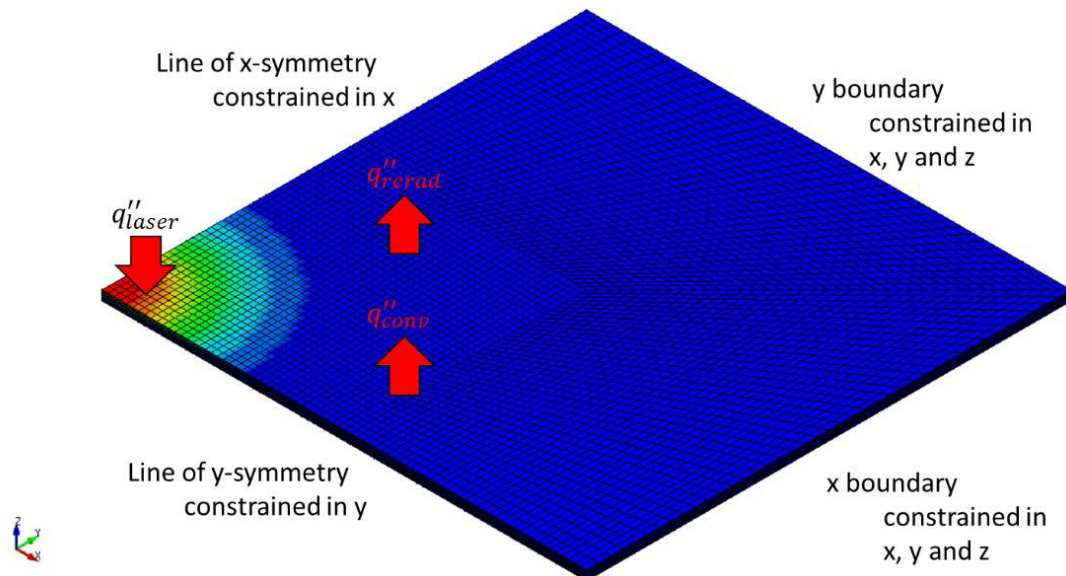


Fig. 4: Diagram of model with boundary constraints and boundary heat fluxes

The laser heat flux boundary condition (Paragraph 4.1) was applied to the front surface of the plate only. The re-radiation (Paragraph 4.2) and convective (Paragraph 4.3) heat flux boundary conditions were applied to both the front and back surfaces of the plate. No heat flux boundary conditions were applied to the boundary or symmetry edges.

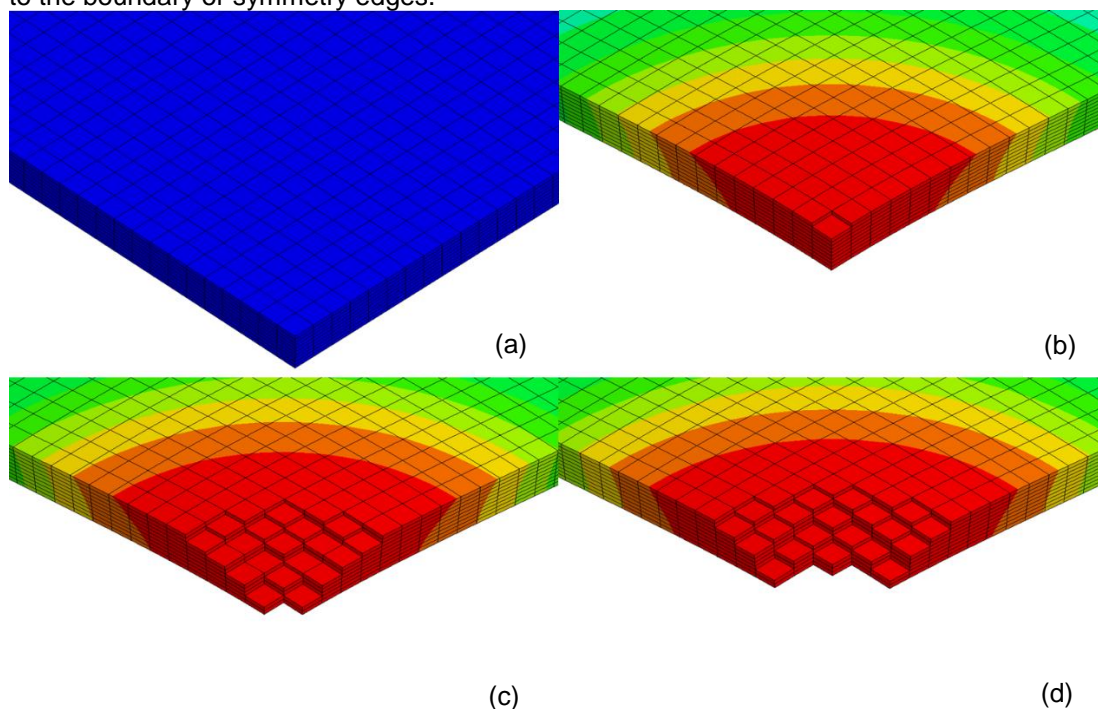


Fig. 5. Temperature contour plot showing element erosion using *MAT_ADD_EROSION when (a) laser heating begins; (b) erosion begins; (c) when plate is fully penetrated; (d) when laser heat heating stops

Fig. 5 displays the behaviour of the model where the most heating is applied. The thermal expansion with the structural material model causes the plate to bend towards the direction that the heating is applied. Once the surface temperature is high enough, the first solid element (at the centre of the front surface) erodes. This erosion process continues symmetrically, until the last, through-thickness element in the centre is also eroded. This is the point at which “time of penetration” or “burn-through time” is defined for the scenario. Because the laser heat flux has not been turned off, the erosion then continues with the hole laterally expanding.

No user intervention was required during the simulations, as the keywords re-applied the heat flux boundary conditions every time an element was deleted.

6 Modelling Results

As a validation exercise, the temperature results and penetration times from all three experiments were compared against the results from the models.

6.1 Temperature Results

The validation results represent data from five thermocouples embedded in different positions on the test plate, positioned at different radial offsets from the centre point (where the laser was aimed). These results have been colour-coded (red, yellow, blue, green and brown), with each colour representing the same gauge position for all three tests. The red thermocouple was located at the front surface, with the others located on the back surface. The yellow and brown thermocouples possessed the same radial position, so they share the same position in the model.

The time to penetrate the plate was also used for validation (discussed later in Paragraph 6.2). In the tests the laser was turned off when penetration occurred, so LCTIM was used with a load curve to turn the laser off in the models at the same point.

The tests were allocated the following numbers: Test 1.1, Test 1.3 and Test 1.4 (Test 1.2 did not provide usable data). The only variable between tests was the total power of the laser beam, Test 1.3 having the lowest laser power and Test 1.4 having the highest laser power.

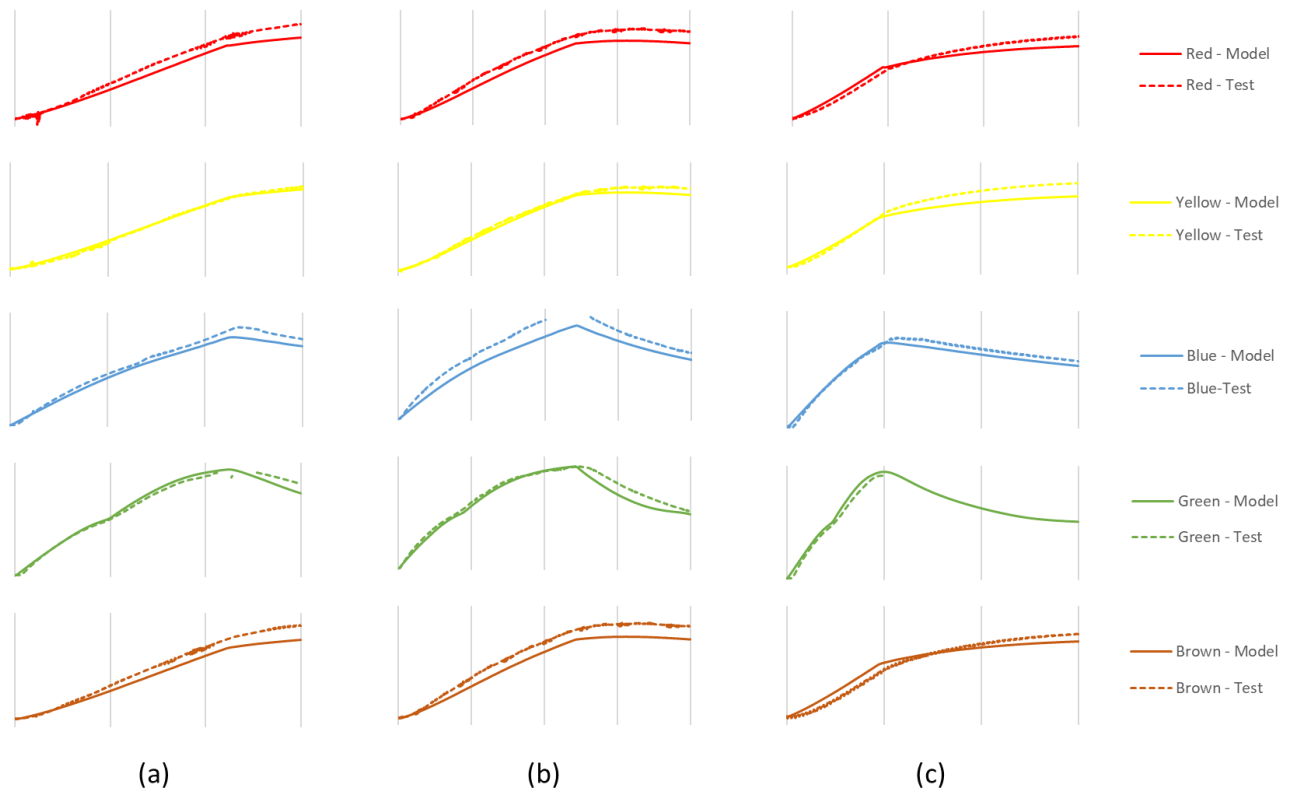


Fig. 6: Comparison of thermocouple and model temperature results for (a) Test 1.1; (b) Test 1.3; (c) Test 1.4

The data from the thermocouple does cut off for some entries, most notable being the blue thermocouple for Test 1.3 and the green thermocouple for Test 1.4. Despite this there is still enough temperature data provided to allow for a comparison.

Test 1.1	Mean Absolute Error (K)
Red	17.90
Yellow	3.40
Blue	47.04
Green	63.27
Brown	17.52

Table 3: Mean Absolute Error values for Test 1.1

Test 1.3	Mean Absolute Error (K)
Red	29.23
Yellow	9.45
Blue	93.69
Green	59.84
Brown	32.14

Table 4: Mean Absolute Error values for Test 1.3

Test 1.1	Mean Absolute Error (K)
Red	12.30
Yellow	18.89
Blue	35.27
Green	53.86
Brown	13.07

Table 5: Mean Absolute Error values for Test 1.4

Tables 3, 4 and 5 show Mean Absolute Error values, providing quantified comparisons of modelled outputs versus thermocouple test data¹. These results, along with the plots shown in Fig. 6, can be used to draw conclusions regarding the relative accuracy of the modelled temperature behaviour.

6.2 Penetration Time Results

For each test, only a single penetration, or “burn-through”, time was provided. These were compared against the modelled results to assess the validity of the numerical method for predicting penetration. The accuracy of modelled penetration times can be expressed using error values, as shown in Table 6, with positive errors indicating over-predictions (relative to experimentally measured values) and negative errors indicating under-predictions.

Test No.	Penetration Time Error (%)
1.1	-3.6
1.3	+3.2
1.4	-11.7

Table 6: Difference between penetration time predictions and recorded values

In the case of Test 1.3, the model had to be run without the laser power being turned off to provide a penetration prediction. This was because full penetration did not occur when this model was setup to exactly match the test parameters.

6.3 General findings

The plots in Fig. 6 show closely matching behaviour between modelled and experimental results, both when laser heating is applied and when laser heating has been turned off. The absolute error results from Table 3, Table 4 and Table 5 also support the conclusion that the modelling technique provides representative temperature predictions.

The comparisons in Table 6 do not show any consistent trends in the differences between the modelled penetration predictions and those recorded in the tests. All predictions are within 12 percent of the time recorded in the tests. These are encouraging results but, because penetration time can only be compared for a single data point for each test, it is not considered as thorough a validation method as comparing the temperature results.

Despite an observable trend of the models to predict temperatures lower than those recorded in the tests, the simulations are considered to show close agreement with the experiments in terms of temperature development and penetration rate for all three tests. Test 1.3 shows the most divergence from the test results as particularly observed in Table 4 with a Mean Absolute Error of 93.69 K, which is significantly higher than any other absolute error values.

¹ Mean Absolute Error = $\frac{\sum_{i=1}^n |T_{model,i} - T_{test,i}|}{n}$

7 Future Development

With the modelling technique validated, the laser modelling capability can be expanded further to include different materials such as aluminium and plastics. The thermal boundary conditions and the rate of penetration can also be developed further to include the effect of different airflows on the surface. More complex scenarios with a moving laser can also be developed.

8 Summary

A new keyword, ***BOUNDARY_FLUX_TRAJECTORY**, has been used in a new technique to replicate a set of laser heating experiments in LS-DYNA. This keyword possesses several unique features that make it suitable for this application; a Gaussian surface heat flux distribution that is easy for a user to define and the ability to continue the heat flux boundary condition to newly exposed elements when existing elements are deleted.

Using additional thermal boundary keywords, three simulations were developed that replicated the important phenomena in a laser heating scenario. These models included thermal behaviour, structural behaviour, and laser-induced penetration alongside each other, with minimal user intervention required to ensure correct operation.

A comparison of the temperature and penetration results from both the experiments and the models shows close agreement, validating the use of this technique to predict material response to heating from high energy lasers.

With the validation successful, future options can include different material types and more complex scenarios.

9 Literature

- [1] Shiva, S., Yadaiah, N., Palani, I. Paul, C. and Bindra, K.: "Thermo mechanical analyses and characterizations of TiNiCu shape memory alloy structures developed by laser additive manufacturing", Journal of Manufacturing Processes, Volume 48, 2019, 98-109
- [2] Bergström, D.: "The Absorption of Laser Light by Rough Metal Surfaces", 2008
- [3] Kaplan, A.: "Fresnel Absorption of 1 μ m- and 10 μ m-laser beams at the keyhole wall during laser beam welding: Comparison between smooth and wavy surfaces", Applied Surface Science, Volume 258, 2012, 3354-3363
- [4] Leitz, K., "Mikro- und Nanostrukturierung mit kurz und ultrakurz gepulster Laserstrahlung", 2013
- [5] Howell, J., Siegel, R., Mengüç, M., "Thermal Radiation Heat Transfer", 5th Edition, 2011
- [6] Shapiro, A., "Using LS-DYNA for Heat Transfer & Coupled Thermal-Stress Problems", LSTC, 2012

© Crown copyright (2021), Dstl. This material is licensed under the terms of the Open Government Licence except where otherwise stated. To view this licence, visit <http://www.nationalarchives.gov.uk/doc/open-government-licence/version/3> or write to the Information Policy Team, The National Archives, Kew, London TW9 4DU, or email: psi@nationalarchives.gov.uk